Diaper Waste Recycling Towards a Triboelectric Nanogenerator based Weather Station: An Innovative Solution for Sustainable Energy Generation

Sayyid Basith[1], Ananthakumar Ramadoss [2], Gaurav Khandelwal [3], George Jacob [4], and Arunkumar Chandrasekhar[1]

[1]Vellore Institute of Technology
[2]CIPET
[3]University of Glasgow
[4]VIT

May 02, 2024

Abstract

The escalating concerns surrounding waste management worldwide and the pressing need for sustainable energy sources have prompted innovative solutions at the nexus of resource recycling and self-powered applications. Diapers are disposed of after use in modern society, and widely available diapers are not environmentally friendly, thus posing a significant threat to the environment. According to the United Nations Environment Programme (UNEP) 2023 report, around 250 million single-use diapers are thrown out daily across the globe. This research presents a pioneering approach to recycling super absorbent polymer (SAP) gels from waste diapers and using them alongside discarded baking sheets to fabricate a maraca-resembled Diaper Waste-based Triboelectric Nanogenerator (DW-TENG). The fabricated DW-TENG is demonstrated for developing a self-powered weather station, enabling real-time wind speed, humidity, and temperature monitoring. The manuscript details the intricate fabrication of the DW-TENG, elucidating design considerations, assembly processes, and the unique roles of SAP powder and baking sheets in the triboelectric energy generation mechanism. In addition, our study quantifies the potential global impact of diaper recycling on energy generation. Based on the calculations, a 4.72 MW power generation is expected yearly, considering the yearly diaper disposal rates. The work highlights the transformative impact of recycling practices for energy generation and represents a promising stride toward a circular and sustainable future.

1. Introduction

The increasing global concern over waste management and the need for sustainable energy sources have propelled innovative approaches toward resource utilization and energy generation[1]. One such creative endeavor involves recycling super-absorbing polymer (SAP) gel obtained from discarded diapers and used non-stick baking sheets for dual purposes, i.e., waste reduction and renewable energy harvesting. This study presented a novel application of triboelectrification principles[2], contact electrification, and electrostatic induction to convert these wastes into a source of self-generated electricity[3,4]. This study focuses on fabricating and applying a novel Diaper Waste-based Triboelectric Nanogenerator (DW-TENG) designed for anemometer functionality and wind energy harvesting.

Diapers are so ubiquitous in modern society that little attention is paid to their impact on the environment. The usage of diapers has become a pervasive and integral aspect of daily life, especially in developed and urbanized regions[5]. Due to their convenience and high absorbency, diapers have emerged as the preferred choice for diapering infants and toddlers. These diapers are meticulously designed with multiple layers

of absorbent materials and waterproof outer layers, ensuring that babies remain dry and comfortable for extended periods, reducing the need for frequent replacements[6]. According to the United Nations Environment Programme (UNEP) 2023 report, around 250 million single-use diapers are thrown away globally daily. Traditionally, these diapers are either incinerated or end up in landfills. According to the Environmental Protection Agency (EPA) 2021 report, it is estimated that one diaper may take up to 500 years to decompose in a landfill[7]. Due to the lack of a proper waste management system, the non-biodegradable diaper components, including polypropylene, polyester, stearyl alcohol, thermoplastic polymer, polyacrylic acid, and fragrance, pose significant environmental and health challenges[8].

Disposed diapers can spread infectious diseases and create a breeding ground for viruses and parasites. It can expose people to different pathogens, including bacteria, viruses, and parasites. Among the bacteria, Escherichia coli (E. coli) is a common inhabitant of the human gastrointestinal tract, with certain strains capable of causing infections and gastrointestinal illnesses[9]. Staphylococcus aureus, another bacterium, can lead to skin infections and respiratory issues[10]. Viruses such as norovirus and rotavirus, both known to affect the gastrointestinal tract, may be present in fecal matter, posing a risk of infection[11]. Parasites like Giardia lamblia and Cryptosporidium, which cause diarrheal illnesses, could also be found in contaminated diapers[12]. Additionally, the presence of fungi, including Candida albicans, may lead to infections, particularly in moist environments[13].

The super absorbent quality of diapers can contaminate groundwater[14]. Rainwater infiltrating landfill waste generates leachate—a liquid mixture of substances from decomposing diapers, including SAP particles[15]. Without proper management, this leachate may permeate the soil, potentially reaching groundwater and introducing SAPs into the water table[16]. Some pathetic visuals of the environmental pollution issues caused by the waste diapers to landfills, oceans, public transport, water resources, agricultural farms, and animal lives are illustrated in Figure 1.

Figure 1. Environmental pollution caused by the disposed diapers: Pollution to a) landfills, b) ocean, c) railway tracks, d) public ponds, e) agricultural farms, and f) public toilets. g) dogs fighting with diapers.

Researchers have indeed proposed several methods for recycling waste diapers, aiming to mitigate the environmental impact of disposable diapers. While previous research has made commendable strides in recycling waste diapers, there are notable challenges and distinctions compared to the proposed work on the Diaper Waste-based Triboelectric Nanogenerator (DW-TENG). Trilokesh et al. have developed a way to recycle baby diaper waste into cellulose and nano cellulose using a chlorine-free approach. They could extract

approximately 25.13% w/w cellulose from used baby diapers[17]. Wang et al. described a method for recycling diaper waste into a magnetic catalyst for the synthesis of glycerol carbonate by calcinating diaper waste above 400°C after impregnating it in the solution of nickel nitrate[18]. Budyk et al. described a method to remove water from disposable diapers and produce a high calorific hydrochar using hydrothermal carbonization[8]. The hydrochars produced had better combustion characteristics and a higher carbon content than dry diapers. Itsubo et al. developed a new technology for the closed-loop recycling of used paper diapers. They evaluated the use of recycled pulp and superabsorbent polymer (SAP) as materials for paper diapers via the environmental impact using the life cycle assessment (LCA) method[19]. Espinosa-Valdemar et al. demonstrated that composting used baby diapers along with yard waste is a feasible and affordable option for their valorization[20].

In contrast, the proposed DW-TENG introduces a novel and sustainable approach by harnessing the mechanical energy from diaper waste for energy harvesting, offering a dual solution to waste management and energy generation. In this work, for the first time, naturally dried super-absorbing polymer gels from sterilized waste diapers are used to fabricate a triboelectric nanogenerator (TENG).

The used baking sheets obtained from landfills serve as the second active layer of the TENG. The non-stick heat-resistant baking sheets are specialized cooking and baking accessories made by coating polytetrafluoroethylene (PTFE) onto a fabric substrate[21]. These sheets feature a smooth, non-stick surface that prevents food from adhering to them during cooking or baking. PTFE coating is renowned for its exceptional non-stick properties, high resistance to heat up to 260°C, and chemical inertness, making it a versatile choice in the kitchen. Many environmental concerns are associated with the dictatorial disposal of PTFE-coated baking sheets in landfills. The PTFE is a synthetic, non-biodegradable fluoropolymer that can generate microplastics if it reaches the environment. The incineration of PTFE or PTFE-coated materials can release toxic fumes and gases, including perfluorinated compounds[22]. Much effort has not been made to recycle PTFE-coated baking sheets. However, several approaches, including hydrothermal treatment[23], solvent-based methods[24], physical separation[25], and depolymerization[26], are proposed to break down or separate PTFE coating from the fabrics. Meanwhile, in this work, these PTFE-coated baking sheets are directly reused for the fabrication of TENG after cleaning and disinfection.

The naturally dried SAP powder and baking sheet were recovered through meticulous sterilization. The SAP powder and baking sheets are then transformed into usable forms as positive and negative triboelectric materials for the fabrication of maraca-shaped DW-TENG. By exploiting the electrostatic properties of SAP powder and baking sheets and based on triboelectrification between these materials, this work was able to collect 259.15 μW of electric power by simple shaking of DW-TENG and build a self-powered mini weather station. This work aligns with the Sustainable Development Goals (SDGs) 3, 7, and 11. This research embarks on a transformative journey to mitigate the environmental impact of disposable diapers. SDG 3's goal of good health and well-being is supported through environmentally friendly practices in waste management. SDG 7's emphasis on affordable and clean energy is met by introducing the DW-TENG as an innovative energy harvester. Furthermore, SDG 11, focusing on sustainable cities and communities, is indirectly addressed by offering a solution for urban waste management[27].

2. Selection of materials

The core materials for fabricating DW-TENG are the disposed diaper gels and baking sheets. The primary function of a diaper is to absorb and retain urine. A typical disposable diaper consists of five layers designed to provide absorbency and leak prevention[28] (Figure 2a). The inner layer (layer 1), which comes into direct contact with the baby's skin, is made of a non-woven fabric that is designed to keep the skin dry and comfortable. Between layers 2 and 3, the distribution layer is filled with cellulose pulps, which help to distribute the absorbed liquid evenly throughout the core, ensuring efficient absorption. The absorbent core between layers 3 and 4 is the core of the diaper, which is filled with SAP and is responsible for absorbing and retaining urine. Finally, it has an outer shell (layer 5) made of waterproof polyethylene to prevent leaks. It serves as a barrier between the absorbent core and the outside environment.

The SAP filled in the absorbent core is a type of cross-linked polymer material, sodium polyacrylate($(C_3H_3NaO_2)_n$or $[\text{-}CH_2\text{-}CH(CO_2Na)\text{-}]_n$), that contains hydrophilic carboxylate (-COO-) functional groups which are responsible for their water-absorbing properties[29] (Figure 2b). The cross-linking involves chemically bonding polymer chains together in a three-dimensional network[30](Figure 2c). When SAPs come into contact with water, the water molecules are attracted to the hydrophilic carboxylate ionic groups, creating osmotic pressure that draws in more water, and this cross-linked structure allows the polymer to expand and swell to form a gel[31]. This swelling with water substantially increases the volume of the SAP polymer gel. However, the chemical composition of the SAP remains unchanged. SAP can absorb up to 400 grams of water per gram of dry polymer[32]. The trapped urine within the gel structure of the SAP is held in place by physical interactions, including hydrogen bonding and van der Waals forces, between the water molecules and the polymer chains[33]. One of the key features of super absorbent polymers is their insolubility in water, which means that once the water is absorbed, it is held within the polymer structure and does not dissolve the polymer. The water remains trapped until external pressure or conditions cause it to be released[34].

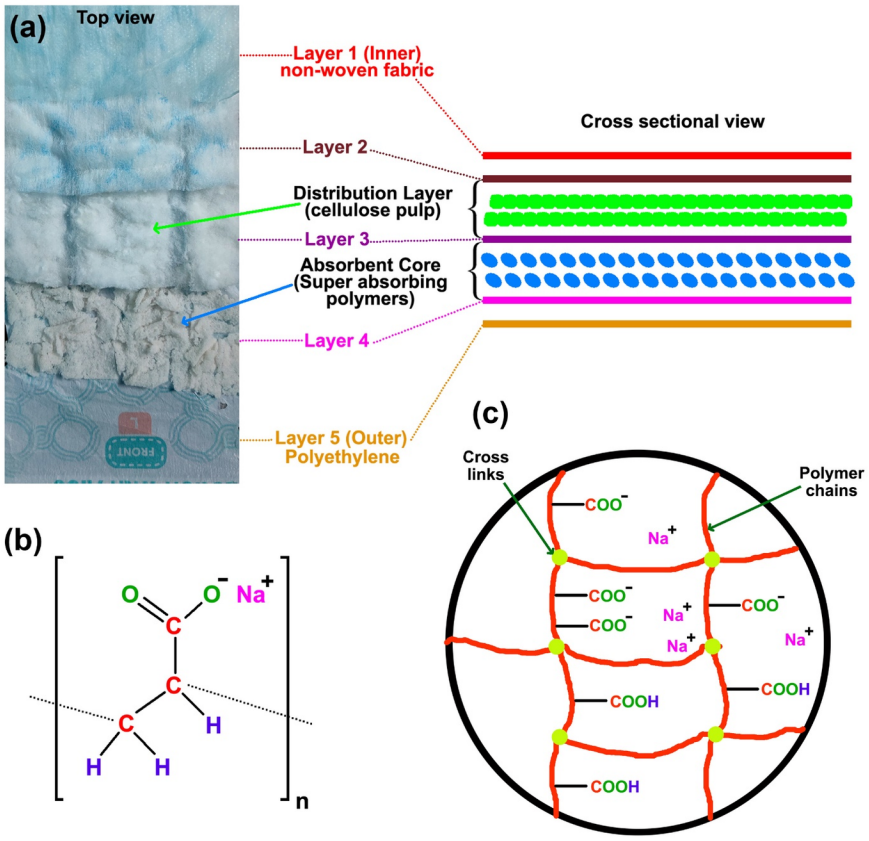

Figure 2. a) Diaper functional layers, b) chemical structure of SAP, and c) cross-linking between functional groups in the super absorbent polymers.

The absorption of urine by SAP is a reversible process[35]. This reversibility allows for the controlled release of trapped water when needed. Recovering SAP from urinated diapers undergoes several steps. Initially, the urinated diapers were soaked in clean water and gently squeezed to release as much liquid as possible. Then, the squeezed SAP gels were collected from the diaper and rinsed with clean water to help remove the urine and contaminants. In the rinsing process, a large volume of water was used to agitate the gel gently. This step was repeated several times until the water ran clearly. Drained the water from the SAP

gel and squeezed it again to remove excess moisture. It was ensured that the applied pressure was low, as high pressure can damage the gel or the polymer chains. Figure S1 shows the cleaning test conducted on urine-soaked diaper gels in the lab with multiple rinses with clean water. After rinsing and squeezing, SAP gel was laid in a well-ventilated area without exposure to sunlight for one week to evaporate the remaining water. A day-by-day analysis of the natural drying of super-absorbing polymer gels for seven days is shown in Figure S2(a-g). Finally, the dried SAP gel was gently crushed to break it into smaller particles to get dried SAP in powder form, as shown in Figure S2(h).

Similarly, baking sheets obtained from landfills were well-cleaned using soapy water and dried in air. Dried SAP powder and baking sheets were sterilized before reuse by soaking them individually in 70% ethanol for 30 minutes, heating them for 20 minutes at 70 °C in a hot air oven, and then exposing them for another 30 minutes to long-wave UV light with a wavelength of 365 nm[36–40].

A direct inoculation sterility testing was performed on the sterilized dried SAP powders and baking sheet in an aseptic room to critically assess whether the sterilized materials were free from contaminating viable microorganisms and to confirm the reusability of the materials towards the DW-TENG fabrication. Initially, a sterile nutrient broth culture media was prepared, and the test samples from both materials were incubated at 37 ^{o}C and monitored continuously for 14 days[41]. Positive and negative controls were used to compare the test results of the materials. In positive control, the medium with added known organisms (Escherichia coli) but without test samples was used to confirm the culture media was capable of microorganism growth. Similarly, a medium without adding both organism and test samples was used in the negative control to verify that any microorganism did not contaminate the culture medium. After 14 days of incubation, turbidity was visualized only in the positive control but not in the negative control or the test sample medium. The sterility test results of the test samples were compared with the positive and negative control samples and confirmed the test negativity on both the sterilized materials, as shown in Figure S3. The lack of turbidity in the test sample media validates the absence of viable microorganisms over the materials. After the sterility test, the naturally dried SAP powder and the baking sheet were reused as integral components of the DW-TENG for energy harvesting and self-powered anemometer application. A complete workflow towards DW-TENG fabrication is graphically illustrated in Figure 3.

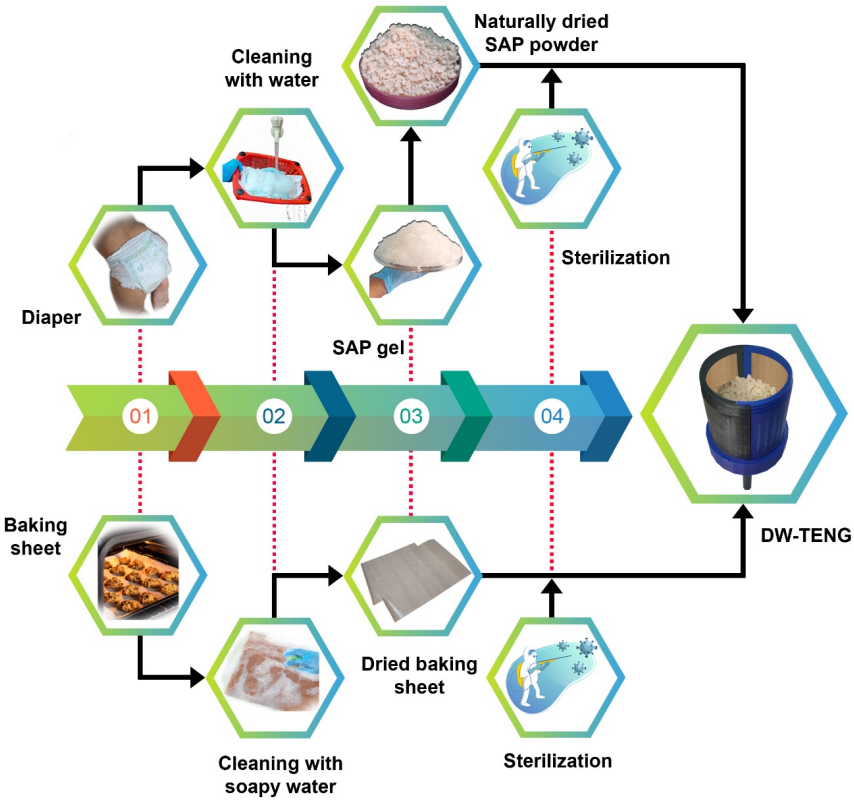

Figure 3. Workflow of DW-TENG fabrication from waste diapers and baking sheets.

3. Material characterization

Various characterization techniques were employed to comprehensively understand the structural and chemical properties of the key components involved in the Diaper Waste-based Triboelectric Nanogenerator (DW-TENG). The detailed characterization sets the foundation for understanding the materials' suitability and performance in the DW-TENG. Fourier-transform infrared spectroscopy (FTIR) and X-ray diffraction (XRD) analyses were conducted on the finally obtained naturally dried SAP powder to characterize its structural and chemical properties and compared its spectra with the FTIR and XRD of the pristine SAP powder collected from the non-urinated and non dumped diapers, as shown in Figure 4(a-b). FTIR spectra analysis of naturally dried SAP powder helps to understand the formation and cross-linking of the sodium polyacrylate superabsorbing polymer. In the spectrum, the peaks observed at 3396 cm^{-1} and 3192 cm^{-1} correspond to O-H hydroxyl and N-H amide stretching, respectively. The absorbance at 2929 cm^{-1} is assigned to the –C-H stretching of the acrylate group. The peak at 1659 cm^{-1} is assigned to the carbonyl (-C=O) group. The absorbance at 1556 $cm^{-1}$is attributed to the sodium acrylate –COONa group, and the peak at 1172 cm^{-1} corresponds to the carboxylate –COO- group. The spectrum of naturally dried SAP matches the FTIR of the pristine SAP, revealing the existence of carboxylate functional groups after drying the SAP powder, and these functional groups are part of the polymer's chemical structure [42]. Drying involves the removal of water from the material, but it does not typically lead to chemical changes in the polymer's backbone or its functional groups.

The broad scattering pattern without distinct peaks in the pristine SAP powder XRD pattern represents sodium polyacrylate's amorphous nature (Figure 4b). This amorphous nature of sodium polyacrylate contributes to its ability to absorb and retain large amounts of water[43]. However, the XRD pattern of naturally dried SAP powder shows the presence of distinct peaks at 32 degrees and 46 degrees, which reveals the for-

mation of some level of crystallinity in the naturally dried SAP. The formation of this crystallinity indicates that the drying process led to the arrangement of more ordered polymer chains, resulting in a partially crystalline structure. The appearance of crystallinity in dried SAP has affected its reabsorption properties.

Fourier Transform Infrared Spectroscopy (FTIR) of the baking sheet, as plotted in Figure 4c, shows the stretches at ~2960 cm^{-1} and ~2852 $cm^{-1}$and the characteristic absorption peaks at wavelengths 1204 cm^{-1}, 1152 cm^{-1}, 635 cm^{-1}, 553 cm^{-1}, and 510 cm^{-1}. The FTIR spectra of the baking sheet match well with the FTIR spectra of PTFE reported in literature[44]. Similarly, the XRD pattern of the baking sheet is shown in Figure 4d, which shows peaks at 18.1°, 31.6°, 36.7°, and 49.3°. These peaks are attributed to the (100), (110), (200), and (210) peaks and match with the XRD spectra of PTFE[45]. Hence, the FTIR and XRD spectra analysis confirmed the presence of PTFE coating over the baking sheet. Energy-dispersive X-ray spectroscopy (EDS) analysis of both the naturally dried SAP powder and pristine SAP powder are shown in Figure 4(e-f), which provide information about their morphology and material elemental composition. EDS confirmed the presence of carbon (C), oxygen (O), and sodium (Na) in both the SAPs. The relative concentrations of material elements in the dried state were 58.12 weight% of Carbon (C) (69.66 Atomic%), 15.01 weight% of Oxygen (O) (13.51 Atomic%), and 26.87 weight% of Sodium (Na) (16.83 Atomic%).

Zeta potential analysis of the naturally dried SAP powder was carried out to understand its surface charge characteristics by creating a stable suspension of the naturally dried SAP powder dispersed in ethanol. A mean zeta potential value of 7.444 mV with a standard deviation of 2.391 mV was observed using a Litesizer 500 Zeta potential analyzer instrument, as shown in Figure 4g. The positive zeta potential indicates a net positive static charge on the surface of the dried SAP powder[46,47]. Hence, dried SAP powder was selected as the triboelectric positive material for DW-TENG fabrication. This observation is supported by the use of polyacrylate balls as triboelectric positive material while fabricating a multidirectional water wave and vibration energy harvester[48]. The baking sheet is coated with PTFE, which is a well-reported negative triboelectric material[49,50]. Scanning electron microscopy (SEM) images of both the naturally dried SAP powder and pristine SAP powder are shown in Figure 4(h-i), and High-resolution optical microscopic visual of the baking sheet and its surface morphology analysis using SEM are given in Figure S4 (a-b). The optical microscopic visual of the baking sheet shows the woven structure of the fabric used to make it, and the plain surface morphology by SEM reveals the presence of PTFE coating over the fabric material.

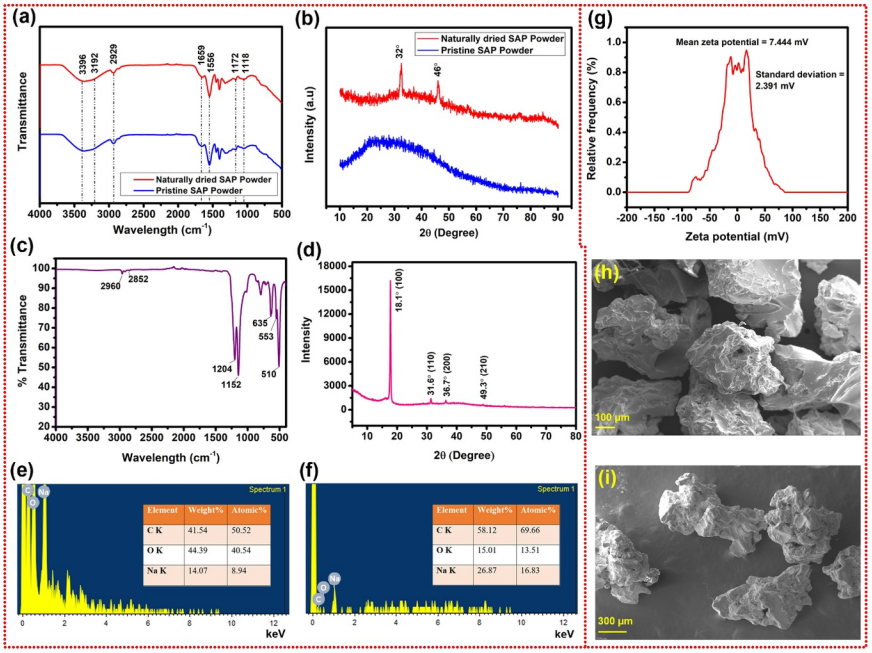

Figure 4. a) FTIR and b) XRD spectrum comparison between naturally dried SAP powder and pristine SAP. c) FTIR and d) XRD spectrum of baking sheet. e) zeta potential plot of naturally dried SAP powder. Scanning electron microscopic (SEM) images of f) pristine and g) naturally dried SAP. Energy-dispersive X-ray (EDX) spectra of h) pristine and i) naturally dried SAP.

4. DW-TENG Fabrication

The diaper waste-based triboelectric nanogenerator (DW-TENG) was fabricated based on the triboelectrification between the naturally dried super absorbing polymer powder and the baking sheet. A cylindrical-shaped housing unit for the DW-TENG, reminiscent of a maraca, was fabricated using polylactic acid (PLA) material using 3D-printing technology. The housing unit comprises five integral components: two vertical half-cylinders, one top cap, one bottom cap, and one holder, as shown in Figure 5a.

The core components in DW-TENG are the dried SAP powder and baking sheet. A pair of disinfected rectangular-shaped baking sheets with dimensions 8 cm x 8.5 cm were taken, and the back side of each was coated with aluminum. The aluminum-coated baking sheets were fixed within each of the vertical half-cylinders of the 3D-printed container (Figure 5b). Here, these pairs of aluminum act as two electrodes for DW-TENG. After fixing these electrode-coated baking sheets, the vertical half-cylinders were joined together, and the lower end was sealed using the bottom cap. The dried and sterilized SAP powder was then filled into the 3D-printed cylindrical container up to approximately 75% of the container volume (Figure 5c). The assembly was completed by attaching the upper cap to the open end of the cylindrical container, effectively enclosing the dried SAP powder within. A cross-sectional view of DW-TENG is shown in Figure 5d. 0.1 mm low gauge wires were used to pull out electrode terminals from each aluminum electrode by inserting a small hole in each half cylinder. These electrode terminals assisted the device in making connections with external circuits and devices. The threaded upper and lower caps seal the container, ensuring a secure and tight fit. Finally, the holder is affixed to the bottom cap, allowing to shake the device manually. When joined, the vertical half-cylinders form a cylindrical container with dimensions of 6.5 cm in diameter and 10.5 cm in height.

As the device was shaken, the SAP powder came into intermittent contact with the baking sheets, initiating charge separation and enabling a continuous flow of electric current through the circuit between the aluminum electrodes. This meticulously designed and fabricated device represents a novel approach to harnessing energy from recycled materials, providing a sustainable and eco-friendly avenue for self-powered applications.

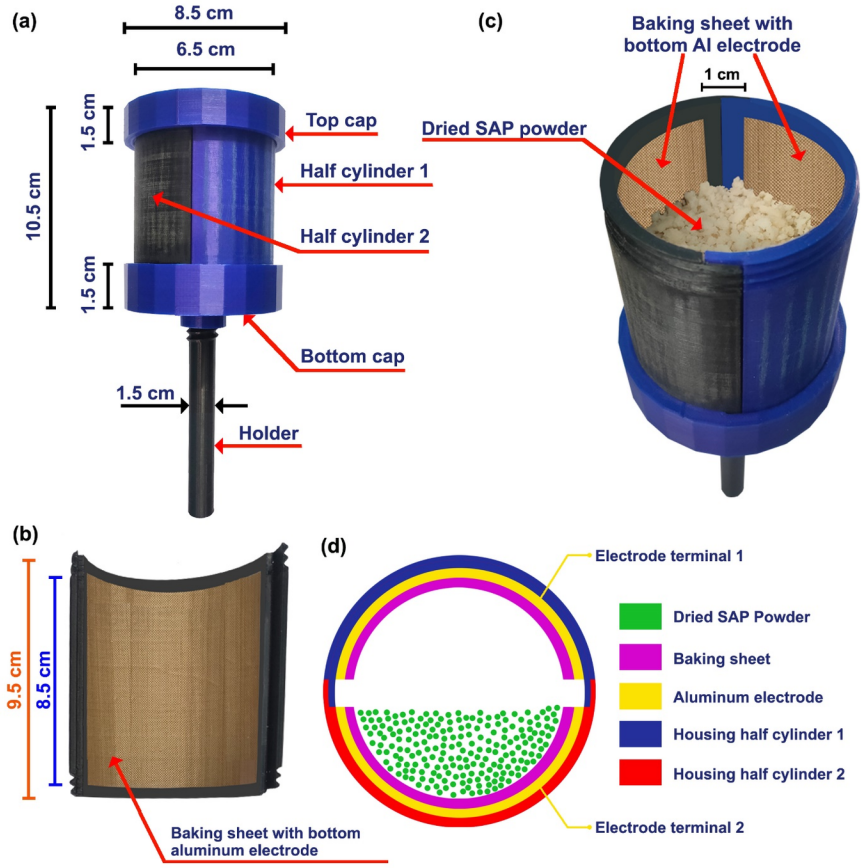

Figure 5. Structure of Diaper Waste-based Triboelectric Nanogenerator (DW-TENG): a) Outside view with dimensions, b) Aluminum-coated baking sheet fixed inside of the vertical half-cylinder, c) DW-TENG filled with dried SAP powder and side walls with aluminum coated baking sheet, and d) cross-sectional view of DW-TENG.

5. Working mechanism

The heart of this innovative energy-harvesting device lies in the synergistic interaction between dried SAP powder and baking sheets. This interaction leverages the principles of triboelectrification and electrostatic induction, facilitating the conversion of mechanical energy into electrical energy. As the device is manually shaken or agitated, the SAP powders come into intermittent contact with the surface of baking sheets within the 3D-printed cylindrical container. This contact initiates a process known as contact electrification. Due to the inherent electrostatic properties of these materials, surface charge transfer occurs between them at the molecular level. The SAP powders, characterized by a positive affinity for electrons, transfer electrons to the surface of baking sheets, which exhibit a negative charge affinity due to the presence of PTFE over the surface. This transfer of electrons results in the accumulation of a positive charge on the SAP powder particles and a negative charge on the baking sheets. While separating SAP from the baking sheet surface, the aluminum attached to the baking sheet becomes induced with positively charged holes due to their contact with the negatively charged baking sheet. At the same time, the counter aluminum electrode becomes negatively charged with electrons. Similarly, the polarity reversal on aluminum electrodes happens when the same SAP powders come into contact with the baking sheet on the other side of the cylinder. In such a way, the cyclic and repeated shaking of the device ensures the alternate polarity changes in the aluminum electrodes, causing a continuous flow of sinusoidal AC electric current through the external circuit established between

the aluminum electrodes (Figure 6(a-f)).

Based on the device model, a COMSOL simulation was modeled by studying electrostatic physics between the materials, and it could visualize the variation in the electric potential distributions on the surfaces of SAP powder and baking sheets for various positions of the diaper powders. The maximum vertical gap between the two baking sheets was set as 7 mm, and the variation in the vertical distance between the lower baking sheet and the powder was considered as a variable parameter "y" so that the powder could move between the vertical distances from 0 to 7mm. The potential distributions at different y values, 0.5 mm, 3.5 mm, and 6.25 mm, are illustrated in Figure 6g. This COMSOL simulations analysis of the model was used to validate the experimental results discussed in the upcoming sessions.

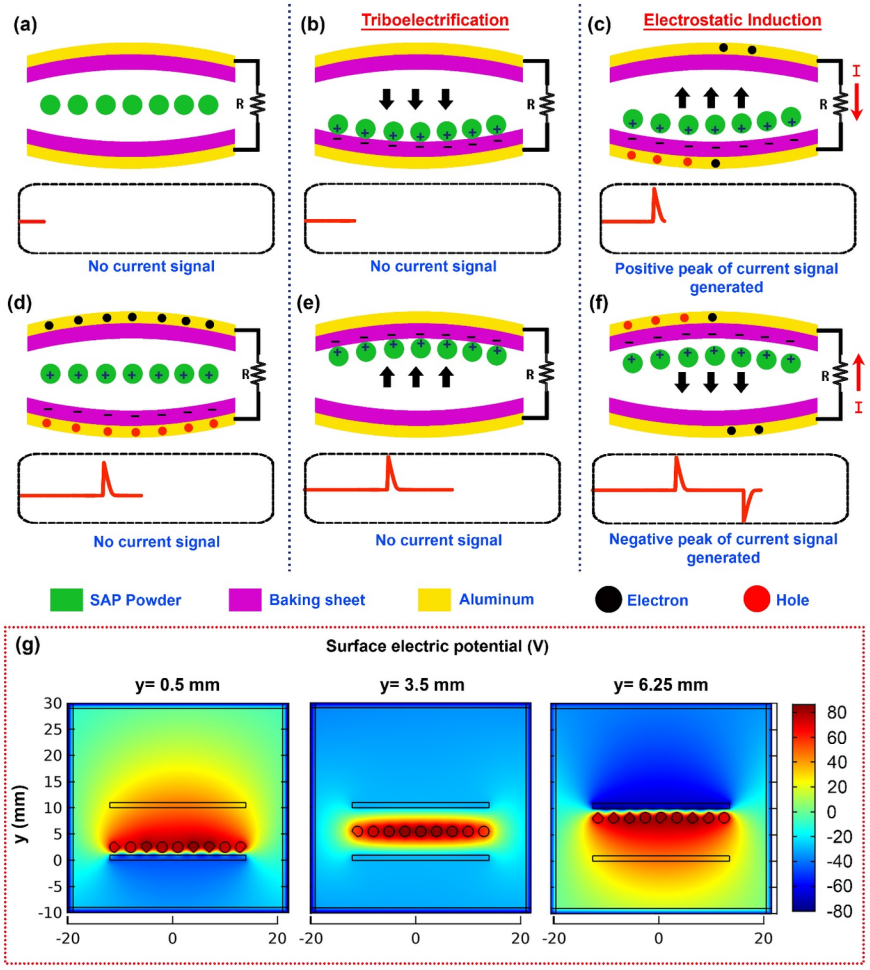

Figure 6. a-f) Electricity generation working mechanism of DW-TENG. g) Surface electric potential distributions obtained by COMSOL simulation at different y positions.

6. Electrical performance

The electrical performance of DW-TENG was rigorously characterized to evaluate its capability for energy harvesting and self-powered applications. The primary focus was on quantifying the electrical parameters, including voltage (V), current (I), and power output (P), under various operating conditions. The device was connected to a linear motor, and electricity generated across the terminals of DW-TENG under mechanical agitations at different operating frequencies of the linear motor was observed. A digital storage oscilloscope

(KEYSIGHT InfiniiVision DSOX2012A) and a picoammeter (Keithley 6485) were used to measure the voltage and current outputs, and data was recorded as a function of time.

As part of device optimization, the electrical performance of DW-TENG was primarily tested by shaking it along the X-X', Y-Y', and Z-Z' axes, as shown in Figure 7a, at a controlled operational frequency of 6 Hz. The voltage and current generated while shaking the device along each axis were observed and plotted, as shown in Figure 7(b-c). DW-TENG shows best electrical output of 110 V and 9 μA along Y-Y' axis vibration due to the maximum contact area between triboelectric materials and the free movement of SAP powders between top and bottom baking sheets. At the same time, the voltage/current along the X-X' and Z-Z' axes were 15 V / 1 μA and 42 V / 3 μA, respectively. Results indicated the capability of DW-TENG for scavenging energy along multi-axis vibrations.

The electrical performances of the DW-TENG along Y-Y' axis were tested and analyzed at different operational frequencies of 2 Hz, 4 Hz, and 6 Hz, as shown in Figure 7(d-e). The results show that voltage and current have a linear relationship with operating frequency. As the frequency was increased to 2 Hz, 4 Hz, and 6 Hz, the corresponding peak-to-peak voltages and currents increased to 35 V/ 2 μA, 72 V/ 6 μA, and 110V/ 9 μA.

The impact of the geometric size of the baking sheet and quantity of SAP powder on the device performance was systematically studied by varying the central angle of the baking sheet arc, adjusting the fill ratio of dried SAP powder inside the cylinder, and measuring the device's voltage at a shaking frequency of 4 Hz along Y-Y' axis. The DW-TENG's response to different baking sheet arc central angles of 80 º, 120 º, and 140 º was evaluated with corresponding arc lengths of 4.5 cm, 6.8 cm, and 8 cm, respectively, by keeping the fill ratio of the SAP powder as 75 %. Figure 7f depicts the observed peak-to-peak voltages as 36 V, 54 V, and 73 V for the respective angles. The increasing trend aligns with expectations, as a larger arc facilitates more significant triboelectric interactions, resulting in higher voltage outputs. This behavior underscores the dependence of the device's response on the area of contact between the SAP powder and the baking sheet.

Further, maintaining a fixed baking sheet arc length of 8 cm and central angle of 140 º, the DW-TENG's electrical performance was analyzed under varying fill ratios of dried SAP powder: 25 %, 50 %, 75 %, and 80 %. The corresponding peak-to-peak voltages were measured as 20 V, 35 V, 79 V, and 60 V, respectively (Figure 7g). The observed increasing trend up to a fill ratio of 75% suggests that the response of the DW-TENG is intricately linked to the area of contact between the SAP powder and the baking sheet. Beyond 75%, the free movement of the SAP powder within the cylinder was obstructed due to the tight occupancy. The restrictive environment led to decreased mobility of the SAP particles, limiting their ability to induce the desired charge separation essential for effective energy harvesting.

Load analysis of the device at 6 Hz frequency was tested, as shown in Figure 7h, to understand the variations in generated voltage and current for a range of load resistances, from 1 to 10^{10} . The instantaneous values of the measured voltage and current were multiplied to get the instantaneous power output of the device. It is observed that the output voltage increases from 0 V to 110 V, and the current decreases from 9 μA to 0 A with increasing load resistance. Maximum power of 259.15 μW was noticed at 10^5 load resistance.

Finally, a capacitor charging analysis of DW-TENG was performed to observe how the device maintains its ability to charge capacitors during repeated operation, which is essential for determining the feasibility of using DW-TENG in practical applications. A 0.1 μF capacitor was connected to DW-TENG through a bridge rectification circuit, and capacitors' charging and discharging were noticed for the continuous shaking of the device at 6 Hz frequency, as shown in Figure 7i and Video S1. It could charge the capacitor up to 7 V within 3 seconds. After the device stopped shaking, the capacitor began to discharge. Video S2 demonstrates a real-time application of the shaking DW-TENG as a power source for a digital thermometer.

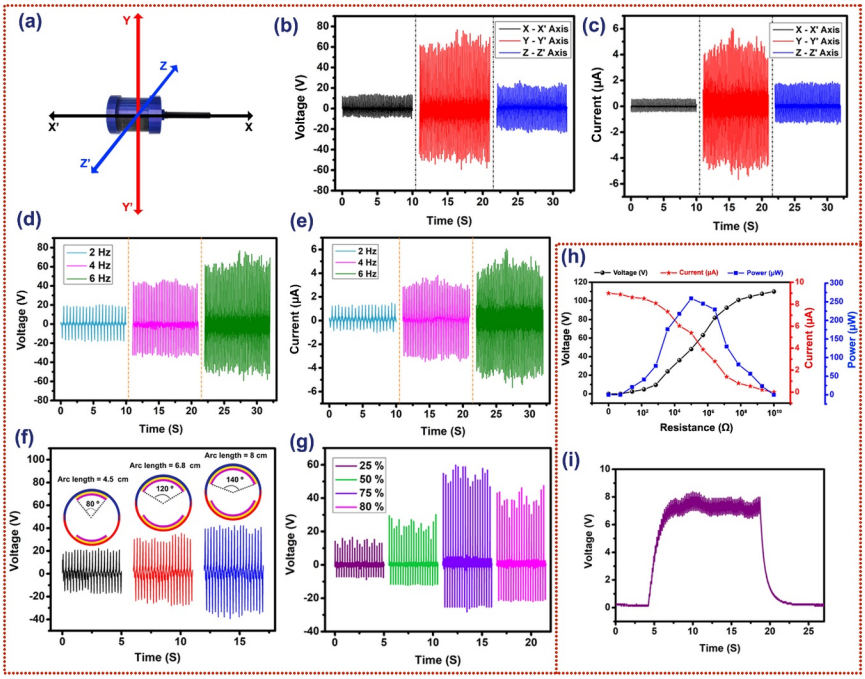

Figure 7. Electrical performances of DW-TENG: a) Axis orientations. b) Voltages and c) Currents obtained during shaking along different axes at 6 Hz frequency. d) Voltages and e) Currents obtained during shaking along Y-Y' axis at different frequencies. Voltages during shaking along Y-Y' axis at 4 Hz shaking frequency with different f) arc lengths of baking sheet and g) fill ratio of dried SAP powder. h) Load analysis and i) capacitor charging test.

7. Real-time applications

7.1 Rotaional wind energy harvester

The DW-TENG represents an innovative approach to energy harvesting, particularly in the realm of rotational energy from wind exposure. In this study, the real-time application of the DW-TENG was demonstrated by mounting it on a supporting framework with the assistance of two ball bearings fixed on the holders attached to the upper and bottom caps, as shown in Figure 8a. A propeller was affixed to one end of the holder, allowing rotation of DW-TENG during wind exposure. Electrode connections were established by extracting low gauge electrode terminals from the inner aluminum electrodes through small holes in the DW-TENG's half-cylinders, and these terminals were then connected separately to two parallel aluminum layers surrounding the cylinder. Outer aluminum connections from the supporting framework were linked to these parallel aluminum layers, enabling the efficient transfer of DW-TENG output to external circuits.

In the experimental exploration of the DW-TENG as a rotational wind energy harvester, a series of tests were conducted to evaluate its performance under various conditions. A speed-adjustable table fan was positioned 2 meters away from the DW-TENG's propeller, simulating wind conditions. Due to the rotation of DW-TENG, SAP powder inside the cylinder slides over through two baking sheets, and due to freestanding operation between the inner SAP power and the baking sheet, a potential difference was created between the two electrodes attached bottom to the baking sheets. The device exhibited voltage and current outputs corresponding to slow (13 V/0.7 μA), medium (39 V/2.7 μA), and fast (64 V/4.9 μA) speeds (Figure 8b-c). This observation underscores the DW-TENG's adaptability to different wind speeds, which is essential for real-world applications. Fast Fourier Transform (FFT) signal analysis provided frequency data for the voltage signals. The frequencies corresponding to slow, medium, and fast speed modes were found to be 2

Hz, 6 Hz, and 10 Hz, respectively (Figure 8d). Converting these frequencies to rotations per minute (RPM) yielded values of 120, 360, and 600 RPM (Figure 8e). This dual functionality positions the DW-TENG as both an energy harvester and a rotational speed sensor.

The DW-TENG's electrode polarity was confirmed by observing a 180^{o} phase shift between voltage waveforms during clockwise and anti-clockwise rotations (Figure 8f). This phase shift validation is crucial for precise integration into electronic systems. The DW-TENG showcased efficient capacitor charging capabilities. Rotating the device at 360 RPM charged a 0.1 μF capacitor to 5 V within 5 seconds (Figure 8g). This rapid charging potential highlights the DW-TENG's suitability for energy storage applications. The energy stored in the charged capacitor was effectively utilized to power practical electronic devices such as a calculator, a digital clock, and 13 series-connected LEDs, as shown in Figure 8(h-j) and Video S3-S5. This real-time demonstration emphasizes the DW-TENG's potential for powering low-energy electronic gadgets.

A comprehensive stability test was conducted to evaluate the stability and durability of the DW-TENG rotational energy harvester. The DW-TENG underwent continuous rotation at 600 RPM for 500 seconds to assess its performance under prolonged operational conditions. The output voltage was consistently measured throughout the test, revealing a peak-to-peak voltage of 64 V (Figure 8k). This result indicates the device's robust stability and sustained performance even during continuous high-speed rotation.

Additionally, the stability test was extended over eight weeks, with separate measurements taken each week, as shown in Figure 8l. Surprisingly, the DW-TENG exhibited a remarkable consistency in output performance, maintaining a peak-to-peak voltage of 64 V throughout each week. This observed stability over an extended timeframe underscores the device's long-term reliability and durability. These findings enhance the confidence in the DW-TENG's performance in real-world applications as a renewable energy harvester, emphasizing its potential for sustainable energy harvesting over prolonged periods. It is crucial in establishing its practical applicability and reliability.

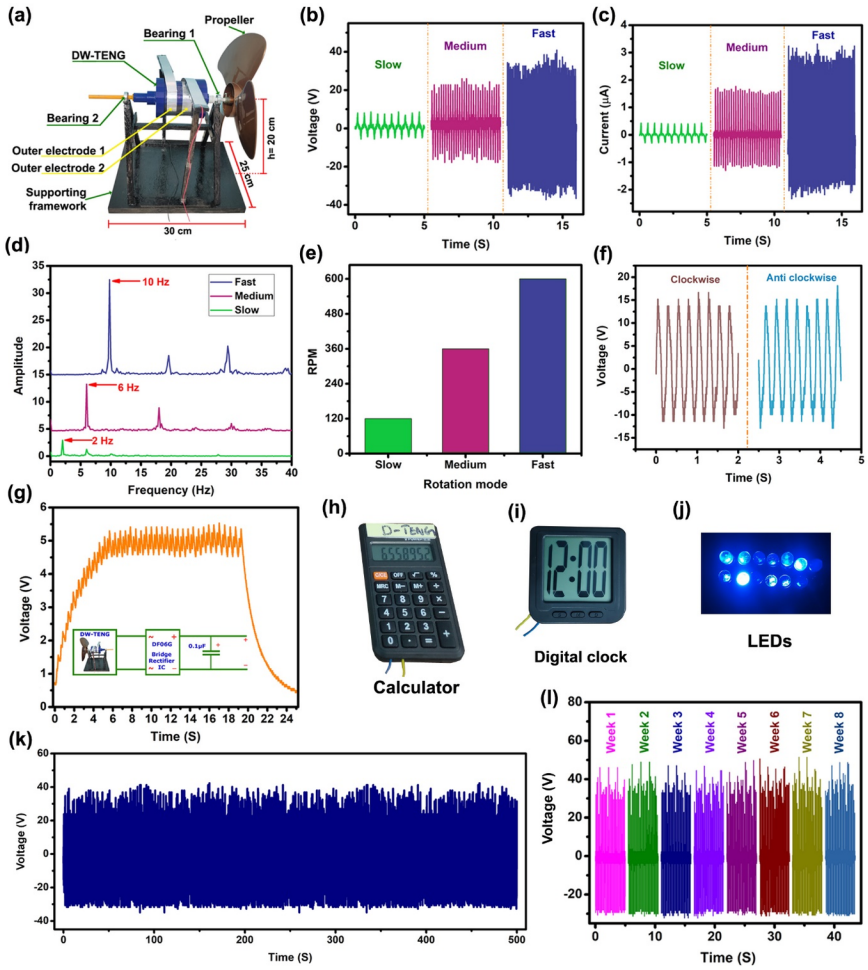

Figure 8. a) DW-TENG rotational energy harvester Axis orientations. b) Voltage, and c) current outputs corresponding to slow, medium, and fast rotations. d) Frequency data obtained by the FFT of the voltages from slow, medium, and fast rotations. e) RPM for slow, medium, and fast rotations. f) Polarity shift observed during clockwise and anti-clockwise rotations. g) Capacitor charging performance at 360 RPM. Real-time powering of low-energy electronic gadgets: h) calculator, i) digital clock, and j) series-connected LEDs. Stability test at 600 RPM for k) continuous 500 seconds and l) successive eight weeks.

7.2 Self-powered anemometer

The successful demonstration of the DW-TENG rotational energy harvester extended its application as a self-powered anemometer to monitor real-time wind speed further by finding a mathematical relationship between the voltage generated from the rotating DW-TENG and the wind speed. A calibrated infrared hotwire anemometer (KUSAM-MECO, Model KM 733), as shown in Figure 9a, was used to measure the wind speed placed near the propeller. At the same time, a digital storage oscilloscope was used to measure the voltage signals generated by the rotating DW-TENG. The infrared (IR) hotwire anemometer is a traditional instrument for measuring wind speed in various applications. It has a sensor probe that houses the hotwire or hot filament heated to a constant temperature. The velocity of the air is then determined based on the cooling effect on the wire. The table fan speed was raised to get infrared hotwire anemometer readings from 0.5 m/s to 10 m/s, and the corresponding voltage outputs from the rotating DW-TENG were recorded and analyzed.

The voltage data corresponding to wind speeds 0.5, 2, 4, 6, 8, and 10 m/s are shown in Figure 9b. It could notice a linear relationship between wind speed and voltage, suggesting that as wind speed increases or decreases, there is a proportional change in the voltage generated by the DW-TENG anemometer. A linear fitting regression analysis was conducted, as in Figure 9c, to obtain a fitting straight-line with equation y = 6.48778x+0.66016 with a coefficient of determination, R^2= 0.99817. The variables x and y represent the wind speed measured by the IR anemometer and the corresponding voltage measured by the oscilloscope, respectively. The R^2 value is a measure of the goodness of linear fit. The equation indicates that for every unit increase in wind speed (x), the voltage (y) increases by a factor of 6.48778, with an additional constant value of 0.66016. This is a common form of a linear equation, where the coefficient 6.48778 represents the slope of the line, and the constant term 0.66016 is the y-intercept.

Later, this relation was used to program a NodeMCU ESP8266 microcontroller to find wind speed directly from the voltage generated by the DW-TENG rotation and to display the live wind speed values through a Blynk IoT cloud platform with the support of the internet. A NodeMCU ESP8266 microcontroller was connected to the DW-TENG rotational energy harvester outputs and interfaced with Blynk cloud support for IoT functionality, as shown in Figure 9d and Video S6-S7. This setup allowed for remote wind speed monitoring through the Blynk application web dashboard, accessible via computer or mobile phone from any location with internet access.

At the same time, the AC sinusoidal voltage output from the DW-TENG rotational energy harvester was rectified and filtered using a DF06G bridge rectifier and a 0.1 μF capacitor (Figure 9d). The resulting DC voltage was utilized to power a QBM Mini digital thermometer hygrometer. This thermometer hygrometer sensor displays the real-time atmospheric temperature and percentage of the relative humidity. It could successfully demonstrate the DW-TENG's ability to monitor wind speed as a self-powered anemometer (Figure 9e) and act as an autonomous power source for a digital thermometer hygrometer. The setup explored its potential as a self-powered weather station by measuring real-time wind speed, humidity, and temperature (Video S8). The interconnected data streams provided a comprehensive overview of environmental conditions.

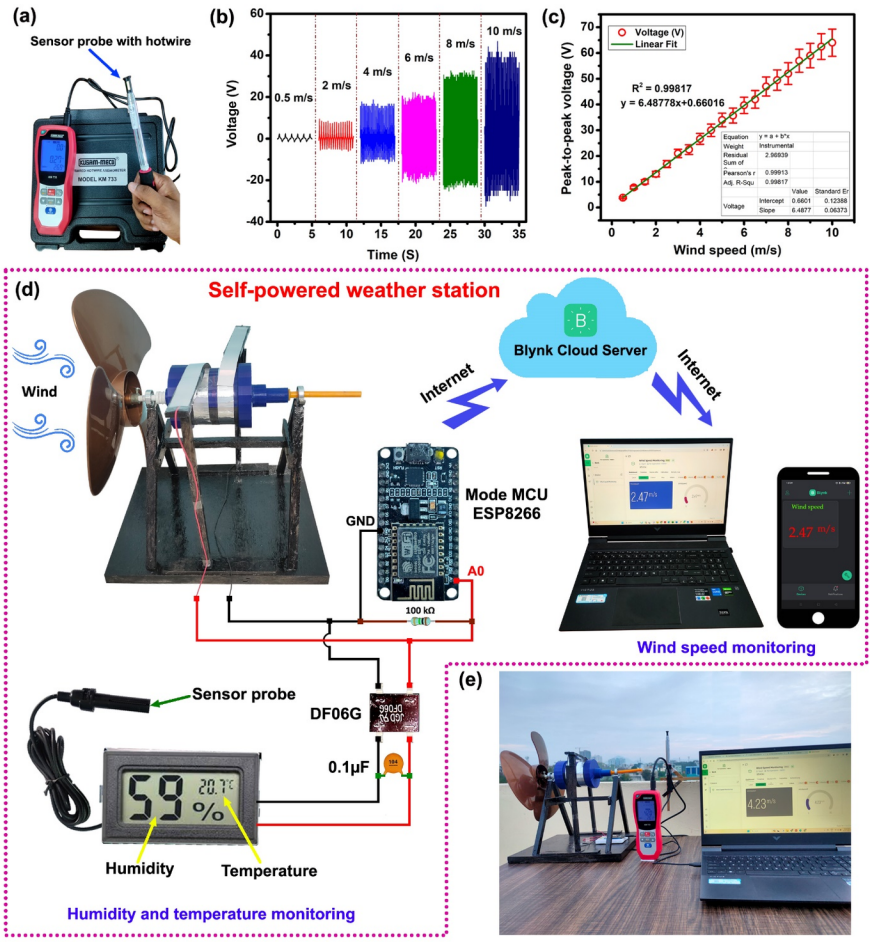

Figure 9. a) Infrared hotwire anemometer. b) Voltage data corresponds to various wind speeds. c) Linear fitting regression analysis of wind speed versus voltage plot. d) weather station: real-time wind speed, humidity, and temperature monitoring. e) Practical outdoor testing of wind speed monitoring.

This study aimed to quantify the potential impact of diaper recycling on global energy generation. With an estimated 250 million single-use diapers discarded daily worldwide, the sheer scale of waste prompted an investigation into harnessing the energy potential within these disposed diapers. The work utilized a mere 150 grams of naturally dried super absorbent polymer (SAP) powder extracted from five waste diapers, generating a noteworthy 259.15 μW of power. This innovative approach presents an opportunity to address both waste management concerns and contribute to renewable energy sources. The daily, monthly, and yearly disposal rates of diapers globally were estimated at 250 million, 7.5 billion, and 91.25 billion, respectively. This staggering quantity underscores the urgency of developing sustainable solutions for diaper waste management.

The power generation potential per diaper was calculated based on the output achieved in the experiment. Using 150 grams of SAP powder from five diapers to produce 259.15 μW, the power per diaper was calculated as

$$Power\ per\ diaper = \frac{259.15\ \mu W}{5} = 51.83\ \mu W$$

Subsequently, the daily, monthly, and yearly electric power generation potentials from globally disposed diapers were determined as

$$\text{Daily power} = \text{Power per diaper} \times \text{Daily disposal rate}$$

$$\text{Daily power} = 51.83\ \mu W \times 250\ million\ =\ 12.95\ kW$$

Similarly,

$$\text{Monthly Power} = 51.83\ \mu W \times 7.5\ billion =\ 388.72\ kW$$

$$\text{Yearly Power} = 51.83\ \mu W \times 91.25\ billion =\ 4.72\ MW$$

The global daily, monthly, and yearly diaper disposal rates and their electric power generation potentials are graphically illustrated in Figure 10 (a-b).

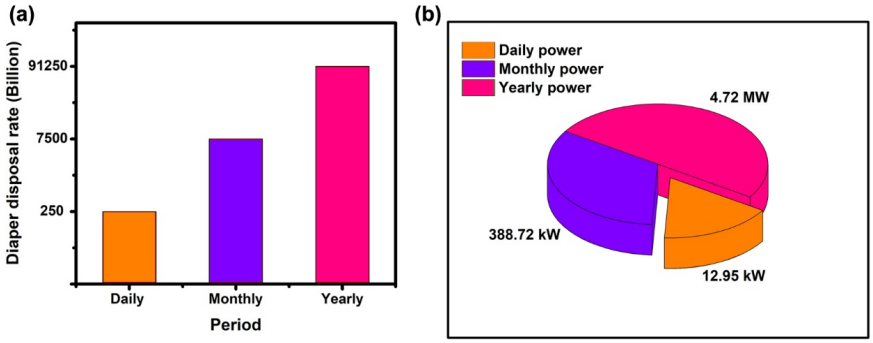

Figure 10. a) Global diaper disposal rates, and b) electric power generation potentials from the disposed diapers.

The results shed light on the significant contribution that diaper recycling could make towards meeting global energy demands. While these calculations provide theoretical insight, the practical implementation and scalability of such methods remain critical considerations for future sustainable energy solutions. The research demonstrates the viability of harnessing energy from diaper waste and emphasizes the urgent need for sustainable waste management practices. By converting diaper waste into a source of self-generated electricity, this work contributes to the ongoing discourse on recycling and renewable energy, offering a promising avenue for addressing environmental and energy challenges globally.

8. Conclusion

The DW-TENG represents an advancement in sustainable weather monitoring and recycling practices. The meticulous fabrication of the DW-TENG, utilizing recycled materials such as SAP powder from disposed diapers, opens avenues for transforming waste into a valuable resource. The device exhibited commendable electrical performance, with notable voltage, current, and power outputs under various operational conditions. Real-time applications demonstrated the DW-TENG's adaptability as a rotational wind energy harvester and a self-powered anemometer, showcasing its potential for practical, real-world implementations. Moreover, the global energy generation potential calculated from disposed diapers emphasizes the transformative impact of recycling practices. With billions of diapers discarded annually, harnessing energy from this

waste source presents a tangible solution to address both waste management and energy challenges. The calculated power generation potentials highlight the significance of such innovative approaches in contributing to global energy demands.

Acknowledgement

An Indian patent has been filed for this work. The authors are grateful to VIT University for providing research facilities and the technical support and discussion of the "Sensor Systems Lab" and "Nanosensors and Nanoenergy Lab" group members.

Conflict of Interest

There is no conflict of interest to declare

References

[1] V. Vedanarayanan, C. Vibhakar, A. Sujaatha, J. K. Chavda, M. Karthik, P. V. Pramila, I. K. Raghavan, *Int. J. Photoenergy***2022** , *2022* , 6711300.

[2] S. A. Basith, A. Chandrasekhar, *Adv. Mater. Technol.***2023** , *8* , 2300495.

[3] A. Chandrasekhar, S. A. Basith, V. Vivekananthan, G. Khandelwal, N. P. M. Joseph Raj, Y. Purusothaman, S. J. Kim, *Nano Energy***2024** , *123* , 109379.

[4] C. Sukumaran, S. Abdul Basith, V. Vivekananthan, S.-J. Kim, A. Chandrasekhar, *Energy Technol.* **2023** , *12* , 2300831.

[5] A. J. Capezza, W. R. Newson, F. Muneer, E. Johansson, Y. Cui, M. S. Hedenqvist, R. T. Olsson, T. Prade, *J. Clean. Prod.***2023** , *387* , 135830.

[6] F. S. F. Ng, S. S. Muthu, Y. Li, P. C. L. Hui, *Crit. Rev. Environ. Sci. Technol.* **2013** , *43* , 1795.

[7] J. Płotka-Wasylka, P. Makoś-Chełstowska, A. Kurowska-Susdorf, M. J. S. Treviño, S. Z. Guzmán, H. Mostafa, M. Cordella, *End-of-life management of single-use baby diapers: Analysis of technical, health and environment aspects* , Vol. 836, **2022** , p. 155339.

[8] Y. Budyk, A. Fullana, *J. Environ. Chem. Eng.***2019** , *7* , 103341.

[9] B. Pakbin, W. M. Brück, J. W. A. Rossen, *Int. J. Mol. Sci.* **2021** , *22* , 9922.

[10] C. Sun, Q. Wang, W. T. Li, D. N. Wen, C. H. Chen, X. Yang, W. Shi, Q. H. Meng, K. H. Yao, S. Y. Qian, *World J. Pediatr.***2020** , *16* , 284.

[11] L. Sai, J. Sun, L. Shao, S. Chen, H. Liu, L. Ma, *Virol. J.* **2013** , *10* , 302.

[12] L. A. Bartelt, E. Attias, J. Black, *Curr. Trop. Med. Reports* **2016** , *3* , 108.

[13] R. Alves, C. Barata-Antunes, M. Casal, A. J. P. Brown, P. van Dijck, S. Paiva, *PLoS Pathog.* **2020** , *16* , e1008478.

[14] C. J. Schenck, T. Y. Chitaka, H. Tyrrell, A. Couvert,*Sustain.* **2023** , *15* , 9478.

[15] D. Roy, A. Azaïs, S. Benkaraache, P. Drogui, R. D. Tyagi,*Rev. Environ. Sci. Biotechnol.* **2018** , *17* , 323.

[16] F. Parvin, S. M. Tareq, *Appl. Water Sci.* **2021** ,*11* , 100.

[17] C. Trilokesh, P. Bavadharani, M. Mahapriyadarshini, R. Janani, K. B. Uppuluri, *Waste and Biomass Valorization* **2021** ,*12* , 4299.

[18] J. Wang, Y. Liang, S. Wang, P. U. Okoye, H. Chen, Y. Zhou, J. Xu, Z. Meng, L. Wang, S. Li, *Int. J. Polym. Sci.* **2020** ,*2020* .

[19] N. Itsubo, M. Wada, S. Imai, A. Myoga, N. Makino, K. Shobatake,*Resources* **2020** , *9* , 34.

[20] R. M. Espinosa-Valdemar, P. X. Sotelo-Navarro, X. Quecholac-Piña, M. Beltrán-Villavicencio, S. Ojeda-Benítez, A. Vázquez-Morillas, *Resour. Conserv. Recycl.* **2014** ,*87* , 153.

[21] M. Sajid, M. Ilyas, *Environ. Sci. Pollut. Res.***2017** , *24* , 23436.

[22] R. Hamaya, Y. Ono, Y. Chida, R. Inokuchi, K. Kikuchi, T. Tameda, C. Tase, K. Shinohara, *J. Med. Case Rep.* **2015** ,*9* , 111.

[23] C. Ouyang, D. Xun, *Coatings* **2022** , *12* , 1649.

[24] A. Ambroziak, P. Kłosowski, *Materials (Basel).***2022** , *15* , 1.

[25] G. Guerrero-Vaca, D. Carrizo-Tejero, Ó. Rodríguez-Alabanda, P. E. Romero, E. Molero, *Materials (Basel).* **2020** ,*13* , 799.

[26] S. Thiyagarajan, E. Maaskant-Reilink, T. A. Ewing, M. K. Julsing, J. Van Haveren, *RSC Adv.* **2022** , *12* , 947.

[27] P. Pradhan, L. Costa, D. Rybski, W. Lucht, J. P. Kropp,*Earth's Futur.* **2017** , *5* , 1169.

[28] S. Dey, M. Purdon, T. Kirsch, H. M. Helbich, K. Kerr, L. Li, S. Zhou, *Regul. Toxicol. Pharmacol.* **2016** , *81* , 183.

[29] M. Mussel, P. J. Basser, F. Horkay, *Gels* **2021** ,*7* , 20.

[30] X. Ma, G. Wen, *J. Polym. Res.* **2020** , *27* , 136.

[31] C. Zhao, M. Zhang, Z. Liu, Y. Guo, Q. Zhang, *ACS Omega***2019** , *4* , 5923.

[32] K. Sharafutdinov, G. Kashevarova, S. KA, *J. Civ. Eng. Res. Technol.* **2021** , *3* , 119.

[33] K. Özan, M. Kanik, S. S. Özer, *J. Appl. Polym. Sci.***2024** , *141* , e54837.

[34] I. Meshram, V. Kanade, N. Nandanwar, P. Ingle, *Int. J. Adv. Res. Chem. Sci.* **2020** , *7* , 8.

[35] T. K. Mudiyanselage, D. C. Neckers, *J. Polym. Sci. Part A Polym. Chem.* **2008** , *46* , 1357.

[36] S. A. Basith, A. Chandrasekhar, *Nano Energy***2023** , *108* , 108183.

[37] Q. H. Nie, X. D. Luo, W. L. Hui, *World J. Gastroenterol.***2003** , *9* , 1139.

[38] C. Meyers, R. Kass, D. Goldenberg, J. Milici, S. Alam, R. Robison, *J. Hosp. Infect.* **2021** , *107* , 45.

[39] J. P. Abraham, B. D. Plourde, L. Cheng, *Rev. Med. Virol.***2020** , *30* , 8.

[40] D. T. Weaver, B. D. McElvany, V. Gopalakrishnan, K. J. Card, D. Crozier, A. Dhawan, M. N. Dinh, E. Dolson, N. Farrokhian, M. Hitomi, E. Ho, T. Jagdish, E. S. King, J. L. Cadnum, C. J. Donskey, N. Krishnan, G. Kuzmin, J. Li, J. Maltas, J. Mo, J. Pelesko, J. A. Scarborough, G. Sedor, E. Tian, G. C. An, S. A. Diehl, J. G. Scott, *PLoS One***2021** , *16* , 1.

[41] A. H. Almehmadi, F. T. Alghamdi, *Cureus* **2022** ,*14* , e25673.

[42] S. H. Saud Hashmi, S. N. Saad Nadeem, Z. A. Zahoor Awan, A. ur R. Adeel ur Rehman, A. A. G. Ahsan Abdul Ghani, *J. Chem. Soc. pakistan* **2019** , *41* , 668.

[43] F. Masuda, Y. Ueda, In *Encyclopedia of Polymeric Nanomaterials* (Eds.: Kobayashi, S.; Müllen, K.), Springer Berlin Heidelberg, Berlin, Heidelberg, **2021** , pp. 1–18.

[44] M. A. Hegazy, H. A. Ezzat, I. S. Yahia, H. Y. Zahran, H. Elhaes, I. Gomaa, M. A. Ibrahim, *Polymers (Basel).* **2022** ,*14* , 1069.

[45] Y. A. Lebedev, Y. M. Korolev, V. M. Polikarpov, L. N. Ignat'ev, E. M. Antipov, *Crystallogr. Reports* **2010** , *55* , 609.

[46] Z. Ge, Y. Wang, *J. Phys. Chem. B* **2017** ,*121* , 3394.

[47] H. Zhang, K. Wang, J. Li, J. Li, R. Zhang, Y. Zheng,*Matter* **2022** , *5* , 1466.

[48] Z. Yuan, C. Wang, J. Xi, X. Han, J. Li, S. Han, W. Gao, C. Pan,*ACS Energy Lett.* **2021** , *6* , 2809.

[49] Z. Zhang, J. Cai, *Curr. Appl. Phys.* **2021** ,*22* , 1.

[50] S. Zhu, Y. Xu, C. Huang, X. Jin, *J. Eng. Fiber. Fabr.***2018** , *13* , 60.

ToC figure